ChemPubSoc Europe

DOI: 10.1002/cctc.201800487

CHEMCATCHEM Communications

Attachment of Iron Oxide Nanoparticles to Carbon Nanotubes and the Consequences for Catalysis

Nynke A. Krans,[a] Ewout C. van der Feltz,[a] Jingxiu Xie,[a] Iulian A. Dugulan,[b] Jovana Zečević,[a] and Krijn P. de Jong*[a]

The attachment of colloidal iron-oxide nanoparticles (designated Fe-NPs) to pristine and surface-oxidized carbon nanotubes (CNTs and CNT-Ox, respectively) was investigated. The loadings of Fe-NPs (size 7 nm) on the CNT and CNT-Ox supports amounted to 3.4 and 2.3 wt.%, respectively; the difference was attributed to weaker van der Waals interactions between the colloidal Fe-NPs and the surface of CNT-Ox. Fischer–Tropsch to olefins (FTO) synthesis was performed to investigate the impact of support functionalization on catalyst performance. Weak interactions between the Fe-NPs and the CNT-Ox support facilitated particle growth and led to substantial deactivation of the Fe/CNT-Ox catalysts. The addition of promoters (Na + S) to Fe/CNT resulted in remarkable activity, selectivity to lower olefins, and stability, making colloidal iron nanoparticles on pristine CNTs a suitable catalyst for FTO synthesis.

Commonly applied catalyst synthesis methods, such as incipient wetness impregnation and precipitation, are often used to obtain supported catalysts for industrial use.[1–3] Controlling the size, composition, and shape of the metal (oxide) nanoparticles, however, is limited with these methods. Colloidal synthesis has been successfully applied to obtain well-defined model catalysts suitable for fundamental studies.[4–6] For example, Fischer–Tropsch to olefins (FTO) is one of the catalytic reactions particularly sensitive to particle size, for which colloidal model systems can be beneficial.[7,8] FTO involves iron-based catalysts and is becoming increasingly important as an alternative to the traditional cracking of crude oil fractions for the production of lower olefins (C2–C4) and aromatics from syngas (CO/H_2).[9–13] In addition, colloidal particles have been shown to be relatively stable and to have catalytic properties that are comparable to those of conventional catalysts, making them interesting model systems for fundamental studies on FTO.[14,15]

[a] N. A. Krans, E. C. van der Feltz, J. Xie, J. Zečević, K. P. de Jong
Inorganic Chemistry and Catalysis
Debye Institute for Nanomaterials Science
Utrecht University
Universiteitsweg 99, 3584 CG, Utrecht (The Netherlands)
E-mail: k.p.dejong@uu.nl

[b] Dr. I. A. Dugulan
Fundamental Aspects of Materials and Energy Group
Delft University of Technology
Mekelweg 15, 2629 JB, Delft (The Netherlands)

Supporting Information and the ORCID identification number(s) for the author(s) of this article can be found under: https://doi.org/10.1002/cctc.201800487.

To increase the activity and selectivity of an FTO catalyst, the addition of promoters is of vital importance, as unpromoted iron catalysts usually show high selectivity towards methane.[16–19] By promoting iron particles with Na and S promoters, low selectivity to methane and high selectivity to olefins can be obtained.[16,18] Moreover, colloidal particles can be promoted by using organic ligand exchange, which specifically targets the promoters on the catalytically active particles.[15,20]

In FTO catalysis, choosing the support material is of importance as well, as strongly interacting supports, such as silica and alumina, can incorporate iron, making reduction and carbidization to the active iron carbide phase difficult.[21–23] Nevertheless, there are many porous carbon materials that can be used as catalyst supports such as activated carbon and graphitic and templated carbon.[24–26] Carbon nanotube (CNT) supports are of growing interest in research owing to their chemical inertness and mesoporosity.[27–29] More importantly, it was found that functionalization of carbon supports suppressed particle growth by the anchoring particles, thereby increasing the stability of the impregnated catalysts.[30–34] The attachment of colloidal particles to support materials has so far not been researched abundantly; however, it has been found that the support material can alter the behavior of the particles during catalysis.[35–38]

In the present work, the impact of carbon surface oxidation on the attachment of colloidal iron-oxide nanoparticles (Fe-NPs) to CNTs and their subsequent promotion with Na + S was investigated. It was found that functionalizing the CNT support by oxidation (CNT-Ox) impeded attachment of the colloidal particles and led to the growth of the nanoparticles, which decreased the catalytic activity. This showed that functionalization of the support is not always beneficial and can have a detrimental effect if colloidal particles are used.

After the synthesis, the size and shape of the Fe-NPs were investigated by transmission electron microscopy (TEM), which showed that 7 nm spherical Fe-NPs with a narrow size distribution were obtained (Figure 1). Subsequently, the impact of oxidation on the acidity and pore volume of the CNT supports was investigated by N_2 physisorption in combination with acid–base titration (Table S1 in the Supporting Information). CNT-Ox displayed significantly higher acidity, and the number of acidic groups was found to be 1.7 nm^{-2}, which indicated successful oxidation. The Fe-NPs were then anchored to both the CNT and CNT-Ox supports, which hereafter are named Fe/CNT and Fe/CNT-Ox. After attachment of the Fe-NPs, sodium and sulfur promoters were added by a ligand-exchange method,[15,20] and the particle size and distribution were stud-

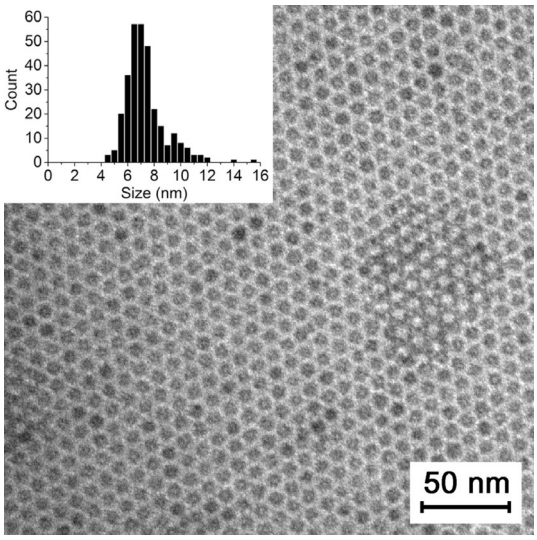

Figure 1. TEM image of well-dispersed 7 nm iron-oxide colloidal nanocrystals sterically stabilized by oleic acid and oleylamine ligands. The inset histogram shows the narrow size distribution.

ied by TEM (Figures 2 and S1); these samples are hereafter referred to as FeP/CNT and FeP/CNT-Ox (P denoting the Na and S promoters). The iron particles were found to be well distributed on the supports, with no indication of aggregation or particle growth. In contrast to the Fe-NPs on the CNT support, the particles on CNT-Ox were less abundant (Figure 2b, d), which implied a weaker interaction between CNT-Ox and the nanoparticles. This was also inferred from particle growth observed during TEM imaging, as this sample had a broader particle-size distribution than the other three samples (Figure S1).

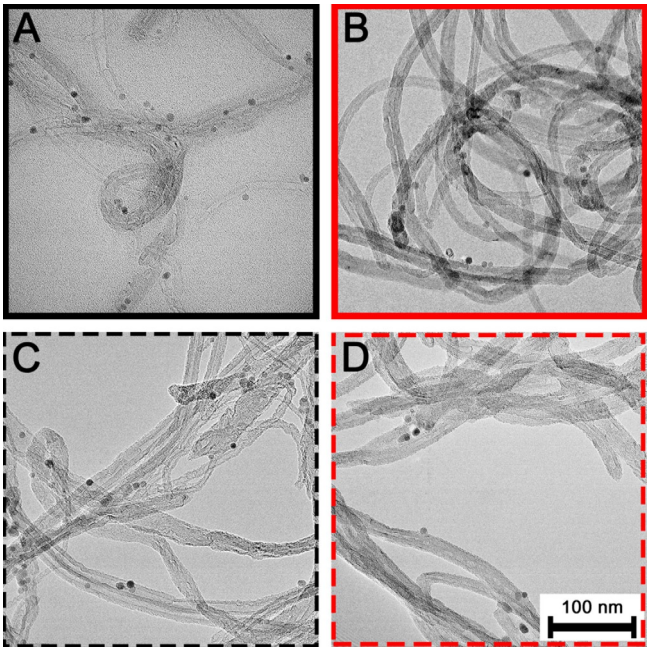

Figure 2. TEM images of the fresh a) Fe/CNT, b) Fe/CNT-Ox, c) FeP/CNT, and d) FeP/CNT-Ox catalysts.

By X-ray diffraction (XRD) analysis (Figure S2) it was observed that all catalysts contained mixed γ-Fe_2O_3 and Fe_3O_4 phases, which is in agreement with our previous findings.[14] Furthermore, inductively coupled plasma atomic emission spectroscopy (ICP-AES) (Table 2) showed that the Fe loading in both the Fe/CNT and FeP/CNT samples was 3.4 wt.%, whereas significantly lower Fe loadings of 2.3 and 2.0 wt.% were detected in Fe/CNT-Ox and FeP/CNT-Ox, respectively. This is in agreement with the TEM results in Figure 2, which reveals a lower number of iron particles attached to the CNT-Ox support, indicating weaker attachment.

The difference in Fe loadings observed by TEM and ICP-AES is tentatively ascribed to different interactions between the Fe-NPs and the supports. This interaction difference is linked to van der Waals forces between the particles and the support that relate to the Hamaker constants, which is larger for the graphitic CNT support than for the graphene-oxide-like CNT-Ox support.[39,40] Additionally, the apparent particle growth during TEM imaging, shown in the histograms in Figure S1, of the Fe-NPs in FeP/CNT-Ox compared to that of the Fe-NPs in Fe/CNT-Ox is explained by particle growth induced by the electron beam as a result of this weaker interaction. Once the ligands are exchanged with smaller Na_2S molecules, the Fe-NP surface can more directly interact with CNT-Ox, and thus, FeP/CNT-Ox is more stable during electron microscopy measurements.

ICP confirmed that ligand exchange was successful, as both promoted catalysts exhibited an increase in Na and S (Table 1).

Table 1. Iron, sodium, and sulfur weight loading on the different supports measured by ICP-AES.[a]

Support material	Fe [wt.%]	Na [wt.%]	S [wt.%]	Atomic ratio Na/S
Fe/CNT	3.4	0.04	< DL	
FeP/CNT	3.4	0.16	0.06	2
Fe/CNT-Ox	2.3	0.05	< DL	
FeP/CNT-Ox	2.0	0.73	0.08	12
CNT	< DL	0.07	0.04	
CNT-Ox	< DL	1.11	0.07	

[a] After correcting for blank CNTs with an average amount of 0.06 wt% Na and 0 wt% S; DL = detection limit.

The Na/S atomic ratio in FeP/CNT was 2, equal to the Na_2S precursor, but the amount of sodium was much higher in the FeP/CNT-Ox catalyst than in the FeP/CNT catalyst. This can be attributed to ion exchange of the Na ions with the surface acidic groups present on CNT-Ox, which suggests that most of the Na ions are present on the support. To verify this hypothesis, we exposed both the CNT and CNT-Ox supports to the same amount of the S and Na promoters used for catalyst preparation. As expected, the amount of sodium was significantly higher in the CNT-Ox support than in the pristine CNT support (Table 1).

The impact of the observed interactions between the iron particles and promoters with the support on catalyst activity, selectivity, and stability for FTO was studied. As known from

previous literature, adding Na + S promoters decreases the hydrogen coverage on the iron surface and thereby the selectivity to methane.[41,42] As expected, the promoted catalysts showed higher iron time yield (FTY) than the unpromoted catalysts (Figure 3), as well as a decrease in the selectivity to CH_4 and an increase in the selectivity to C2–C4 olefins (Table 2).

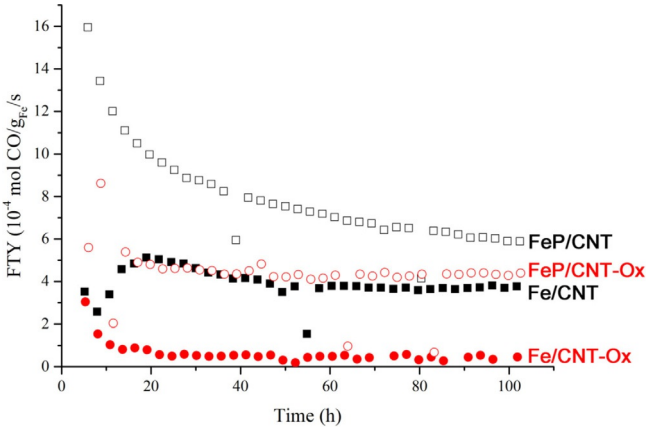

Figure 3. Iron-time yields (FTYs) for CNT-supported iron catalysts: Fe/CNT (■), FeP/CNT (□), Fe/CNT-Ox (●), and FeP/CNT-Ox (○).

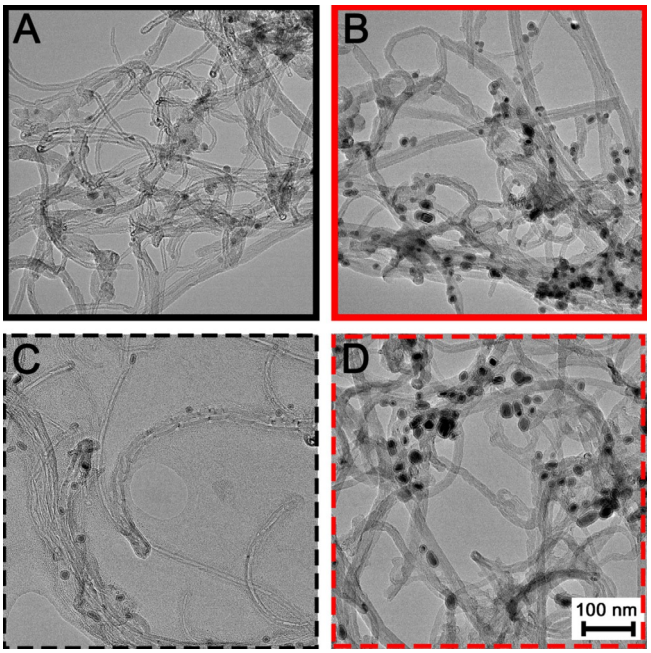

Figure 4. TEM images of the spent a) Fe/CNT, b) Fe/CNT-Ox, c) FeP/CNT, and d) FeP/CNT-Ox catalysts.

Table 2. Catalytic activity and selectivity of pristine and oxidized support materials for the FTO reaction.[a]

Support material	FTY [10^{-4} mol g_{Fe}^{-1} s^{-1}]	Selectivity [%C] CH_4	C_2–C_4 olefins	C_{5+}	CO_2
Fe/CNT	3.5	40	26	10	28
Fe/CNT-Ox	0.5	N.D.	N.D.	N.D.	N.D.
FeP/CNT	6.0	11	48	34	38
FeP/CNT-Ox	4.5	8	51	37	38

[a] Reaction conditions: 10 bar (1 bar = 0.1 MPa, 340 °C, H_2/CO = 2, time on stream = 100 h. The FTY of the promoted samples clearly show an increase as a result of the Na + S promoters, as well a decrease in the selectivity to methane and an increase in the selectivity to lower olefins and C_{5+}. The CH_4, C_2–C_4 olefins, and C_{5+} selectivities are given with CO_2 excluded. N.D. = not determined.

However, after 100 h on stream, FeP/CNT-Ox displayed lower iron-normalized activity than FeP/CNT, most possibly due to particle growth during catalysis. Moreover, Fe/CNT-Ox showed no activity after the first 20 h, which led to results that contrasted those in the literature. Although the literature points to the beneficial effect of functionalized groups on CNTs for impregnated iron catalysts,[30] it is clear that if colloidal Fe-NPs are used that the effect is adverse. The spent catalysts were analyzed by TEM, as shown in Figure 4. Owing to conversion of the Fe-NPs into the active carbide phase, core–shell particles had formed and were observed in all catalysts, albeit mostly in the promoted ones.[17] From quantitative analysis of the TEM images, it appears that 35% of such core–shell particles were present in Fe/CNT, whereas Fe/CNT-Ox had 75%. This nicely matched the Mössbauer spectroscopy results (Tables S2 and Figure S3) that the same amount of Fe-NPs was converted into the ε-$Fe_{2.2}C$ and χ-Fe_5C_2 phases, which are considered active in FTO.[43] Interestingly, it was observed that only the core–shell particles had grown, which suggested that carbidization coincided with particle growth. Even though Fe/CNT-Ox was inactive after only 20 h on stream, this catalyst seemed to have more activated particles than Fe/CNT. Further investigations will be necessary to explain the cause for such low inactivity.

Both promoted catalysts were fully carbidized, as indicated by Mössbauer, which matched the TEM results showing 100% core–shell particles. More importantly, CNT-Ox supported catalysts showed noticeable particle growth (Figures 4b and S4b,d), most probably as a consequence of the weaker attachment of the Fe-NPs to the oxidic surface, which led to sintering during the FTO reaction. These results are comparable to previous results from our group for impregnated catalysts on an ordered mesoporous carbon support, for which poor catalytic activity was attributed to growth and encapsulation of the particles by carbon.[34] Finally, these findings indicate that attaching colloidal particles to an oxidized carbon nanotube support resulted in deactivation during the catalytic reaction owing to the poor interaction of the Fe-NPs with the surface.

In conclusion, colloidal iron-oxide nanoparticles (Fe-NPs) were attached to two supports, namely, pristine carbon nanotubes (CNTs) and oxidized CNTs (CNT-Ox), to investigate the impact of the attachment and the addition of a promoter on catalyst activity, selectivity, and stability for Fischer–Tropsch to olefins (FTO) catalysis. It was found that the oxidation of the support led to a lower weight loading of the Fe-NPs because of a weaker interaction between the CNT-Ox support and the particles. The addition of Na + S promoters resulted in a highly active catalyst for pristine CNTs, whereas particle growth impeded FeP/CNT-Ox activity. We hypothesized that the lower ac-

tivity of the CNT-Ox supported catalysts was due to insufficient attachment of the Fe-NPs to the support, which caused particle growth under the FTO conditions. Finally, it was concluded that colloidal Fe-NPs interacted differently on the surface-oxidized carbon supports than on the nonoxidized supports as a result of different van der Waals forces and that this can have a big impact on catalyst performance.

Experimental Section

Details of the fabrication of the iron-oxide nanoparticles, the attachment of the Fe-NPs to the CNTs, oxidation of the CNT support by liquid-phase oxidation, and the addition of the Na_2S promoter by ligand exchange can be found in articles previously published by our group.[14,15,27] Synthesis methods and characterization can be found in the Supporting Information.

Acknowledgements

We acknowledge the European Research Council, EU FP7 ERC Advanced Grant no. 338846. H. C. de Waard (UU) is acknowledged for ICP-AES measurements. Willem Kegel and Alfons van Blaaderen are acknowledged for useful discussions

Conflict of interest

The authors declare no conflict of interest.

Keywords: alkenes · iron · nanoparticles · nanotubes · supported catalysts

[1] P. Munnik, P. E. De Jongh, K. P. De Jong, *Chem. Rev.* **2015**, *115*, 6687–6718.
[2] F. C. Meunier, *ACS Nano* **2008**, *2*, 2441–2444.
[3] J. Ma, Z. Zhu, B. Chen, M. Yang, H. Zhou, C. Li, F. Yu, J. Chen, *J. Mater. Chem. A* **2013**, *1*, 4662.
[4] Y. Yin, A. P. Alivisatos, *Nature* **2005**, *437*, 664–670.
[5] G. A. Somorjai, F. Tao, J. Y. Park, *Top. Catal.* **2008**, *47*, 1–14.
[6] C.-J. Jia, F. Schüth, *Phys. Chem. Chem. Phys.* **2011**, *13*, 2457.
[7] J. P. Den Breejen, P. B. Radstake, G. L. Bezemer, J. H. Bitter, V. Frøseth, A. Holmen, K. P. De Jong, *J. Am. Chem. Soc.* **2009**, *131*, 7197–7203.
[8] H. M. Torres Galvis, J. H. Bitter, T. Davidian, M. Ruitenbeek, A. I. Dugulan, K. P. De Jong, *J. Am. Chem. Soc.* **2012**, *134*, 16207–16215.
[9] I. Wender, *Fuel Process. Technol.* **1996**, *48*, 189–297.
[10] M. Boudart, M. A. McDonald, *J. Phys. Chem.* **1984**, *88*, 2185–2195.
[11] E. De Smit, B. M. Weckhuysen, *Chem. Soc. Rev.* **2008**, *37*, 2758–2781.
[12] J. L. Weber, I. Dugulan, P. de Jongh, K. P. de Jong, *ChemCatChem* **2018**, *10*, 1108–1112.
[13] H. M. Torres Galvis, K. P. De Jong, *ACS Catal.* **2013**, *3*, 2130–2149.
[14] M. Casavola, J. Hermannsdörfer, N. De Jonge, A. I. Dugulan, K. P. De Jong, *Adv. Funct. Mater.* **2015**, *25*, 5309–5319.
[15] M. Casavola, J. Xie, J. D. Meeldijk, N. A. Krans, A. Goryachev, J. P. Hofmann, A. I. Dugulan, K. P. De Jong, *ACS Catal.* **2017**, *7*, 5121–5128.
[16] H. M. Torres Galvis, J. H. Bitter, C. B. Khare, M. Ruitenbeek, A. I. Dugulan, K. P. de Jong, *Science* **2012**, *335*, 835–838.
[17] J. Xie, H. M. Torres Galvis, A. C. J. Koeken, A. Kirilin, A. I. Dugulan, M. Ruitenbeek, K. P. De Jong, *ACS Catal.* **2016**, *6*, 4017–4024.
[18] M. Oschatz, N. Krans, J. Xie, K. P. De Jong, *J. Energy Chem.* **2016**, *25*, 985–993.
[19] Y. Cheng, J. Lin, K. Xu, H. Wang, X. Yao, Y. Pei, S. Yan, M. Qiao, B. Zong, *ACS Catal.* **2016**, *6*, 389–399.
[20] A. Nag, M. V. Kovalenko, J. S. Lee, W. Liu, B. Spokoyny, D. V. Talapin, *J. Am. Chem. Soc.* **2011**, *133*, 10612–10620.
[21] C. H. Zhang, H. J. Wan, Y. Yang, H. W. Xiang, Y. W. Li, *Catal. Commun.* **2006**, *7*, 733–738.
[22] J. Y. Park, Y. J. Lee, P. K. Khanna, K. W. Jun, J. W. Bae, Y. H. Kim, *J. Mol. Catal. A* **2010**, *323*, 84–90.
[23] K. R. P. M. Rao, F. E. Huggins, V. Mahajan, G. P. Huffman, V. U. S. Rao, B. L. Bhatt, D. B. Bukur, B. H. Davis, R. J. O'Brien, *Top. Catal.* **1995**, *2*, 71–78.
[24] F. Rodríguez-Reinoso, *Carbon* **1998**, *36*, 159–175.
[25] Y. Yang, K. Chiang, N. Burke, *Catal. Today* **2011**, *178*, 197–205.
[26] J. Zhu, A. Holmen, D. Chen, *ChemCatChem* **2013**, *5*, 378–401.
[27] T. O. Eschemann, W. S. Lamme, R. L. Manchester, T. E. Parmentier, A. Cognigni, M. Rønning, K. P. De Jong, *J. Catal.* **2015**, *328*, 130–138.
[28] P. Serp, M. Corrias, P. Kalck, *Appl. Catal. A* **2003**, *253*, 337–358.
[29] W. Chen, Z. Fan, X. Pan, X. Bao, *J. Am. Chem. Soc.* **2008**, *130*, 9414–9419.
[30] H. J. Schulte, B. Graf, W. Xia, M. Muhler, *ChemCatChem* **2012**, *4*, 350–355.
[31] J. L. Figueiredo, *J. Mater. Chem. A* **2013**, *1*, 9351–9364.
[32] M. S. Shafeeyan, W. M. A. W. Daud, A. Houshmand, A. Shamiri, *J. Anal. Appl. Pyrolysis* **2010**, *89*, 143–151.
[33] C. Alegre, M. E. Gálvez, E. Baquedano, E. Pastor, R. Moliner, M. J. Lázaro, *J. Catal.* **1989**, *115*, 98–106.
[34] M. Oschatz, J. P. Hofmann, T. W. van Deelen, W. S. Lamme, N. A. Krans, E. J. M. Hensen, K. P. De Jong, *ChemCatChem* **2017**, *9*, 620–628.
[35] B. H. Juárez, M. Meyns, A. Chanaewa, Y. Cai, C. Klinke, H. Weller, *J. Am. Chem. Soc.* **2008**, *130*, 15282–15284.
[36] D. Park, S. M. Kim, S. H. Kim, J. Y. Yun, J. Y. Park, *Appl. Catal. A* **2014**, *480*, 25–33.
[37] B. Ritz, H. Heller, A. Myalitsin, A. Kornowski, F. J. Martin-Martinez, S. Melchor, J. A. Dobado, B. H. Juárez, H. Weller, C. Klinke, *ACS Nano* **2010**, *4*, 2438–2444.
[38] K. An, S. Alayoglu, T. Ewers, G. A. Somorjai, *J. Colloid Interface Sci.* **2012**, *373*, 1–13.
[39] J. L. Li, J. Chun, N. S. Wingreen, R. Car, I. A. Aksay, D. A. Saville, *Phys. Rev. B* **2005**, *71*, 1–6.
[40] M. J. McAllister, J. L. Li, D. H. Adamson, H. C. Schniepp, A. A. Abdala, J. Liu, M. Herrera-Alonso, D. L. Milius, R. Car, R. K. Prud'homme, I. A. Aksay, *Chem. Mater.* **2007**, *19*, 4396–4404.
[41] J. Xie, J. Yang, A. I. Dugulan, A. Holmen, D. Chen, K. P. De Jong, M. J. Louwerse, *ACS Catal.* **2016**, *6*, 3147–3157.
[42] H. M. Torres Galvis, A. C. J. Koeken, J. H. Bitter, T. Davidian, M. Ruitenbeek, A. I. Dugulan, K. P. De Jong, *Catal. Today* **2013**, *215*, 95–102.
[43] J. W. Niemantsverdriet, A. M. Van der Kraan, W. L. Van Dijk, H. S. Van der Baan, *J. Phys. Chem.* **1980**, *84*, 3363–3370.

Manuscript received: March 23, 2018
Revised manuscript received: April 24, 2018
Accepted manuscript online: April 30, 2018
Version of record online: May 28, 2018